THE JOURNAL OF PHYSICAL CHEMISTRY C

Article

pubs.acs.org/JPCC

Surface Chemistry and Lithium-Ion Exchange in $LiMn_2O_4$ for the Electrochemical Selective Extraction of LiCl from Natural Salt Lake Brines

Florencia Marchini, Diego Rubi,[†] Maria del Pozo, Federcio J. Williams, and Ernesto J. Calvo*

INQUIMAE, Facultad de Ciencias Exactas y Naturales, Pabellón 2, Ciudad Universitaria, AR-1428 Buenos Aires, Argentina

Supporting Information

ABSTRACT: We report on the surface and bulk chemistry of $Li_xMn_2O_4$ ($0 \leq x \leq 1$) spinel oxide electrode for the selective extraction of LiCl from natural salt lake brines using an electrochemical method based on $LiMn_2O_4$ (LMO) lithium intercalation electrode and polypyrrole (PPy) reversible chloride electrode. Both the surface composition and insertion/release of Li ions into/from the crystal structure have been studied with pulsed laser deposited (PLD) thin $Li_xMn_2O_4$ films and composite LMO/carbon black electrodes. Cyclic voltammetry (CV), XPS/UPS, XRD, chrono-amperometry, and galvanostatic intermittent titration technique (GITT) experiments in model $LiNO_3$ solutions and natural brines from Salar de Olaroz (Jujuy, Argentina) have been used. Repetitive CV and GITT experiments showed reversible extraction/intercalation of Li ions in LMO with high selectivity and electrode stability in natural brine, while PPy is reversible to chloride ions. Chronoamperometry for time-bound diffusion in small nanocrystals with interference of concentration profiles yielded $D_{Li}^{+} \sim 10^{-10}$ $cm^2 \cdot s^{-1}$. Photoelectron spectroscopy showed Mn/O surface stoichiometry close to 1:2 and initial 1:1 Mn^{IV}/Mn^{III} ratio with Mn^{III} depletion during oxidation at 1.1 V vs Ag/AgCl and recovery of surface Mn^{III} after reduction at 0.4 V. Coadsorption of Na^+ was detected which resulted in slower ion exchange of Li ions, but there was no evidence of Na^+ intercalation in the Mn oxide electrode.

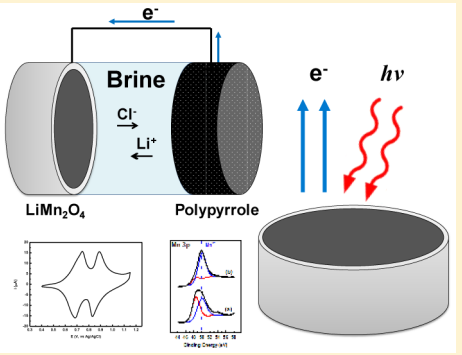

INTRODUCTION

The importance of lithium metal and lithium salts is rapidly increasing due to multiple applications in diverse fields such as batteries, pharmaceuticals, coolants, aluminum smelting, ceramics, enamels and glasses, nuclear fuels, etc. Lithium compounds are required for hybrid electric vehicles, such as the cathode materials and electrolyte salts. Lithium manganese oxide, lithium iron phosphate, or mixed metal oxides such as lithium cobalt nickel manganese oxide can be used as active materials for ion battery cathodes.

Lithium compounds, e.g., lithium chloride or lithium carbonate, are typically obtained from lithium-containing minerals such as spodumene (lithium aluminum silicate) or by extraction from Li-containing brines from high altitude salt lakes such as the Salar de Atacama in Chile, Salar de Uyuni in Bolivia, and Salar del Hombre Muerto in Argentina.

The current soda lime method for the extraction and purification of lithium from high-altitude salt lakes relies on brine evaporation and fractional crystallization of Li, Na, K, and Mg chlorides. After evaporation in open shallow ponds to concentrate the salts, Li_2CO_3 is precipitated by addition of Solvay, and the lithium-depleted brine is discarded. The chemical process is relatively simple; however, it has a high environmental impact since it takes place at 4000 m above sea level where water is scarce and ecosystems are fragile. The extraction process profoundly alters the water balance, introduces chemicals in the environment, and generates large volumes of NaCl and $MgSO_4$ waste. Therefore, there is a need for methods and devices to extract lithium efficiently at low cost from brines and from low concentration sources while having a reduced impact on the environment.

Different electrochemical methods have been reported: Kanoh[1,2] reported the insertion of lithium ions into an electrochemical Pt/λ-MnO_2 cell; La Mantia and co-workers[3−5] introduced the concept of an entropic cell based on battery $LiFePO_4$ cathode and Ag/AgCl reversible chloride anode for the selective recovery process; a similar λ-MnO_2/Ag battery was reported by Lee and co-workers[6] for artificial brine or λ-MnO_2/activated carbon hybrid supercapacitor;[7] and Hoshino proposed an electrodialysis method using ionic liquid-based membrane technology.[8,9] Fast and efficient chemical redox insertion of lithium ions into solid $FePO_4$ has been reported by Owen and co-workers,[10] while the $LiFePO_4/FePO_4$ electrochemical cell with an anion exchange membrane was reported for the extraction of Li from brine.[11]

An alternative electrochemical method for the extraction of lithium chloride from brine or seawater has been proposed recently.[12] In this electrochemical method, which is fast and

Special Issue: Kohei Uosaki Festschrift

Received: November 30, 2015
Revised: January 18, 2016

DOI: 10.1021/acs.jpcc.5b11722
J. Phys. Chem. C XXXX, XXX, XXX−XXX

efficient and has low environmental impact and low energy consumption, brine containing lithium is in contact with a lithium-deficient $Li_xMn_2O_4$ (LMO) cathode and a chloride-reversible poly(pyrrole) (PPy) anode. Upon applying a potential difference of less than 1 V, insertion of lithium ions at the LMO electrode and exchange of chloride at the PPy electrode take place simultaneously with high selectivity. In a second step the electrodes are in contact with a lithium recovery electrolyte, and the electrode potential is reversed, so that lithium releases at the LMO anode and the PPy cathode releases chloride ions. During the lithium chloride uptake, only Li^+ ions are selectively intercalated at the cathode and Cl^- ions exchanged at the anode, while the release of LiCl into the recovery electrolyte takes place in the second step.

Herein we report physicochemical studies of surface and bulk changes of $Li_xMn_2O_4$ ($0 \leq x \leq 1$) battery electrodes in $Li_xMn_2O_4$/polypyrrole cells in contact with natural brine and $LiNO_3$ electrolyte for the selective extraction of Li ions. Surface Mn^{IV}/Mn^{III} redox sites, coadsorption of Na^+, and intercalation of Li^+ have been studied during insertion/extraction cycles with photoelectron spectroscopy (XPs, UPS), X-ray diffraction (XRD), and electrochemical techniques.

EXPERIMENTAL SECTION

$LiMn_2O_4$ was obtained from Sigma-Aldrich and also prepared by a ceramic process (firing and grinding) from $MnCO_3$ and Li_2CO_3, and the resulting mixed oxide was characterized by XRD and SEM. Thin $LiMn_2O_4$ films were grown by pulsed laser deposition (PLD) using a Q-switched Spectra Physics laser with λ = 266 nm and a repetition frequency of 10 Hz at a temperature of 650 °C and an oxygen pressure of 0.1 mbar. The laser fluency was fixed at 2 J/cm^2. After growth, a soft annealing was performed at the growth temperature, at an oxygen pressure of 13 mbar. The films resulted were single phase and polycrystalline with thickness estimated between 100 and 250 nm.

Some LMO electrodes were prepared by casting a slurry of $LiMn_2O_4$ (80% w/w), 10% PVDF, and 10% Vulcan carbon X-72 (Cabbot Corp.) dispersed in *N*-methyl pyrrolidone onto flat carbon Poco and dried at 105 °C.

The electrolytes were 0.1 M $LiNO_3$, 0.1 M $LiNO_3$ + x M $NaNO_3$ (x = 0.1, 1 M), and natural brine from Salar de Olaroz in the province of Jujuy, Argentina. The chemical composition of the natural brine was analyzed by ICP resulting in Na^+ 115.600 ppm (5 M NaCl), K^+ 10.780 ppm (0.28 M KCl), Mg^{2+} 2.618 ppm, Li^+ 975−1280 ppm (0.18 M LiCl), B 1.440 ppm, with a dynamic viscosity of 2.077 Cp, density 1.2710 g·cm^{-3}, and conductivity 0.1735 S·cm^{-1}.

The chloride-reversible polypyrrole counter electrode was obtained by electrochemical polymerization of 0.1 M pyrrole on large surface area platinum mesh (Goodfellow PT008710) in 1.2 M HCl in water under potential control at 0.8−1 V vs Ag/AgCl, 3 M KCl, during 1 h (see Supporting Information).

XRD measurements were performed over a 1.3 cm^2 stainless steel cast with LMO ink ($LiMn_2O_4$, Carbon Vulcan and PVDF; 80:10:10% w/w ratio) after being polarized for 2 h either at 0.4 or 1.1 V vs Ag/AgCl.

The reference electrode was a Ag/AgCl, 3 M KCl (0.21 V vs NHE and 3.21 V vs Li/Li$^+$), and all potentials herein are quoted with respect to that reference electrode. All electrochemical experiments were performed with an Autolab PGSTAT 30 potentiostat (Autolab, Ecochemie, Holland) with Nova 1.10 software in PTFE three-electrode undivided cells.

XPS and UPS measurements were performed within an ultrahigh vacuum chamber (UHV; base pressure <5 × 10^{-10} mbar)[13] equipped with a transfer system built in our laboratory, which allows rapid and controlled transfer of the sample between the UHV environment and the atmospheric (Ar) liquid electrochemical environment and the possibility to carry out ex-situ photoelectron spectroscopic measurements on samples that were initially clean in UHV and were never exposed to the laboratory atmosphere, thus having full spectroscopic knowledge of the surface before and after each electrochemical experiment.

Electrochemical measurements were carried out in a three-electrode cell, which consists of a platinum sheet as counter electrode, Ag/AgCl (in KCl 3 M) as the reference electrode, and a $LiMn_2O_4$ film over a stainless steel substrate, as the working electrode. The $LiMn_2O_4$ sample was initially Ar^+ sputtered at 3 keV and annealed at 623 K in subsequent cycles until no significant C 1s signal was detected by XPS.

Each experiment involved the transfer of the initially spectroscopically clean sample from the UHV environment to the electrochemical cell without being exposed to the laboratory atmosphere at any moment. To perform the electrochemistry, a meniscus was formed with the $LiMn_2O_4$ sample touching the aqueous electrolyte solution. After each electrochemical process, the solution was removed, and the sample was extensively rinsed with Mili-Q water, dried under a constant flow of Argon, and transferred back to the analysis chamber. The analysis chamber is equipped with a SPECS UHV spectrometer system which consists of a 150 mm mean radius hemispherical electron energy analyzer and a nine channeltron detector. XP spectra were acquired on grounded conducting substrates at a constant pass energy of 20 eV using a Mg Kα (1253.6 eV) source operated at 12.5 kV and 20 mA at a detection angle of 30° with respect to the sample normal. No charge compensation was necessary, and no differential charging features were observed given that we have measured sufficiently thin films on grounded conducting substrates. Atomic ratios were calculated from the integrated intensities of core levels after instrumental and photoionization cross-section corrections. UPS spectra were acquired using a He I radiation source (21.2 eV) operated at 100 mA with normal detection at a constant pass energy of 2 eV.

RESULTS AND DISCUSSION

Cyclic Voltammetry. Figure 1 shows a SEM image of the PLD $LiMn_2O_4$ thin film with homogeneous distribution of nanocrystals with average size 100 nm.

Figure 2 depicts a typical cyclic voltammetry at low scan rate (2 mV·s^{-1}) of $LiMn_2O_4$ electrode in contact with 0.1 M $LiNO_3$ (Figure 2a) and natural brine containing 5 M NaCl (Figure 2b), respectively. A qualitatively similar current potential curve is observed in both cases with two sets of anodic, A1 and A2, and two cathodic peaks, C1 and C2, in the potential range between 0.5 and 1.1 V, which are comparable to those reported for $LiMn_2O_4$ in nonaqueous EC/DMC 1 M $LiPF_6$ electrolyte[14−16] which have been ascribed to a two-step delithiation−litiation process between $LiMn_2O_4$ and λ-MnO_2.[15,17] These peaks correspond to the Li-ion insertion/extraction due to the simultaneous redox change in the Mn^{III}/Mn^{IV} in the spinel host structure. We have restricted the potential window to 0.4−0.6 and 1.0−1.2 V in order to keep the lithium stoichiometry within the $0 \leq x \leq 1$.

DOI: 10.1021/acs.jpcc.5b11722
J. Phys. Chem. C XXXX, XXX, XXX−XXX

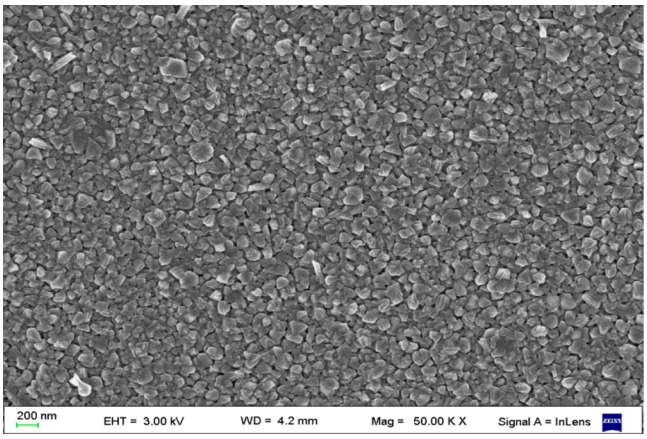

Figure 1. Scanning electron micrograph of a PLD $LiMn_2O_4$ thin-film laser deposited on stainless steel.

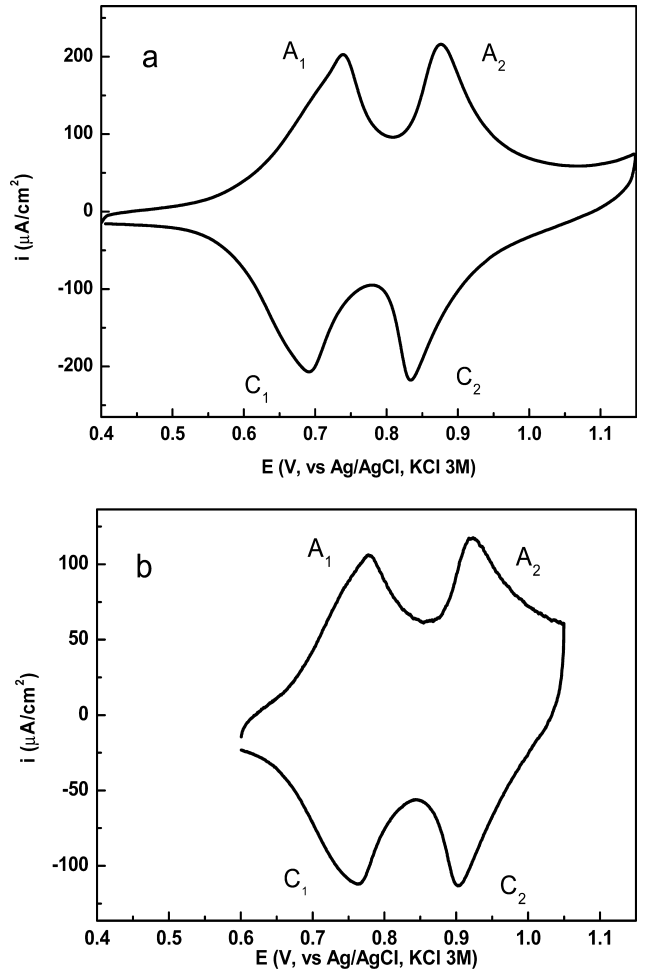

Figure 2. Cyclic voltammetry of PLD $LiMn_2O_4$ electrode in (a) 0.1 M $LiNO_3$ and Pt counter electrode and (b) natural brine with PPy counter electrode at 2 $mV{\cdot}s^{-1}$.

It is to be noted that the peaks in the case of brine as electrolyte are slightly shifted to higher potentials, i.e., 0.91/0.77 V (or 4.13/3.99 in the Li/Li^+ scale) and 0.85/0.72 V (or 4.07/3.94 in the Li/Li^+), respectively, and the redox charge (14−15 $mC{\cdot}cm^{-2}$) is smaller in brine than in 0.1 M $LiNO_3$ (44 $mC{\cdot}cm^{-2}$). This seems to be related to a kinetic effect due to sodium-ion coadsorption on the oxide surface as shown by XPS (see below) or by changes in ion activity due to different ionic strength.

$LiMn_2O_4$ is a stable phase with half lithium content in the discharge curve from λ-MnO_2 to $Li_2Mn_2O_4$.[18,19] The mixed oxide, $LiMn_2O_4$, has a spinel structure (space-group $Fd3m$), and the unit cell contains 56 atoms: A cubic close-packed array of oxygen ions occupying the 32e sites; 16 Mn ions are located in the octahedral 16d sites (MnO_6); and 8 Li ions are in the tetrahedral 8a sites.[14]

Lithium ions can be inserted in the λ-MnO_2 cubic phase and extracted from $LiMn_2O_4$ in aqueous solutions by a topotactic Li^+ insertion reaction within the cubic symmetry with isotropical expansion of the cell.[1,20] Using an electrode reversible to chloride ions it is possible to extract Li^+ and Cl^- ions from brine solutions by adjusting the redox state of manganese ions in the oxide lattice.

In analogy to the $LiMn_2O_4$ positive lithium-ion battery electrode in nonaqueous electrolyte, the available positions for lithium insertion into λ-MnO_2 are tetrahedral 8a sites in the spinel structure.[14] There are two sets of nonequivalent 8a sites which can be occupied in $Li_xMn_2O_4$ (with $x \leq 1$), respectively, by four lithium ions, each leading to two peaks in the cyclic voltammetry. The transition occurs at $Li_{0.5}Mn_2O_4$ composition.

The electrode reactions at the electrode/electrolyte interfaces during the extraction and release of LiCl from brine within the cubic LMO structure are

$$x\mathrm{Li}^+(\mathrm{brine}) + \mathrm{Li}_{1-x}\mathrm{Mn}^{\mathrm{III}}_{1-X}\mathrm{Mn}^{\mathrm{IV}}\mathrm{O}_2 + x\mathrm{e}^-(\mathrm{cathode}) \leftrightharpoons \mathrm{LiMn}^{\mathrm{IV}}\mathrm{Mn}^{\mathrm{III}}\mathrm{O}_4 \quad (1)$$

while at the chloride reversible electrode, oxidation of polypyrrole occurs with simultaneous uptake of chloride anions to compensate the excess positive charge in the polyions.[21,22]

$$x\mathrm{Cl}^-(\mathrm{brine}) + x\mathrm{PP}^0(\mathrm{anode}) \rightleftharpoons x[\mathrm{PP}^+\mathrm{Cl}^-] + x\mathrm{e}^-(\mathrm{anode}) \quad (2)$$

$LiMn_2O_4$ is half way between cubic λ-MnO_2 (Mn^{IV}) and tetrahedral $Li_2Mn_2O_4$ ($Mn^{III/IV}$) oxides. Further lithium-ion insertion in the $LiMn_2O_4$ phase is known to cause Jahn−Teller distortion as a consequence of unstable Mn^{3+} (d^4) formation in an octahedral environment, which leads to a first-order transition with a change from cubic to tetragonal symmetry to form $Li_2Mn_2O_4$ which takes place close to 3 V vs Li/Li^+

$$\mathrm{LiMn}^{\mathrm{IV}}\mathrm{Mn}^{\mathrm{III}}\mathrm{O}_4 + x\mathrm{Li}^+ + x\mathrm{e} \rightleftharpoons \mathrm{Li}_{1+x}\mathrm{Mn}^{\mathrm{III}}_{1+x}\mathrm{Mn}^{\mathrm{IV}}_{1-x}\mathrm{O}_4 \quad (3)$$

At this point, since 16c octahedra share faces with the 8a tetrahedra, the Li ions in the 8a tetrahedral sites are displaced into the vacant 16c sites, causing the phase transition. Complete filling of the 16c positions yields a composition corresponding to $Li_2Mn_2O_4$.

Therefore, the overall electrochemical process can be described as

$$x\mathrm{Li}^+(\mathrm{brine}) + x\mathrm{Cl}^-(\mathrm{brine}) + \mathrm{Li}_{1-x}\mathrm{Mn}^{\mathrm{III}}_{1-X}\mathrm{Mn}^{\mathrm{IV}}\mathrm{O}_2 + x\mathrm{PP}^0 \leftrightharpoons \mathrm{LiMn}^{\mathrm{IV}}\mathrm{Mn}^{\mathrm{III}}\mathrm{O}_4 + x[\mathrm{PP}^+\mathrm{Cl}^-] \quad (4)$$

Initially, the fully lithiated $LiMn_2O_4$ is subject to anodic treatment in an electrolyte with low or nil Li^+ concentration before the uptake of LiCl from brine solution under cathodic polarization. In chloride-containing solutions the counter electrode of PPy is reversible to chloride ions and avoids

DOI: 10.1021/acs.jpcc.5b11722
J. Phys. Chem. C XXXX, XXX, XXX−XXX

chlorine evolution which otherwise occurs on a Pt counter electrode.

During the overall process aqueous lithium ions are expected to adsorb on the LMO electrode surface losing their hydration shells and becoming intercalated into the spinel crystal structure by slow ion diffusion in the solid. The knowledge of the surface composition, coadsorption of lithium, and other ions is therefore relevant for the overall extraction/insertion process.

Surface Composition. We are interested in the study of the surface composition of the $Li_xMn_2O_4$ as a function of the state of charge during delithiation/lithium insertion, and for that purpose we have employed photoelectron spectroscopy. The surface composition of LMO electrodes has been studied as a function of the state of charge by an electrochemical experiment coupled to an UHV transfer system[13] that allows electrochemical experiments and then to transfer the sample for photoelectron spectroscopic studies without exposing it to the atmosphere, thus avoiding surface contamination.

X-ray photoelectron spectroscopy of the manganese−oxygen systems has been described elsewhere.[23] We have studied the Mn 2p, Mn 3s, Mn 3p, O 1s, Li 1s, and Na 1s spectra for PLD $Li_xMn_2O_4$ thin films under different electrochemical treatments during delithiation and Li^+ insertion processes. Most XPS studies of LMO have been reported in the Mn 2p region because it has the highest photoionization cross section and hence a larger signal. However, the Mn 2p XPS signal is complex with multiple splitting of the core lines and a rather small peak shift as a function of the Mn oxidation state.[24] The valence state of Mn in mixed-valence oxides can also be obtained by XPS using the Mn 3s core-level electrons. This core level shows multiple splitting, and the binding energy difference between the high- and low-spin components can be correlated to the relative content of Mn(III) ions.[25,26] However, when the two Mn oxidation states are present, broadening of the low-spin component is observed, and thus the multiple splitting binding energy difference cannot be easily determined (see Supporting Information).

Therefore, we have determined the oxidation state of surface Mn ions using the Mn 3p doublets at 50.2 and 48.6 eV for Mn(IV) and Mn(III), respectively.[23,24,27−29] Here we should note that the Mn 3 $p_{3/2}$ and 3 $p_{1/2}$ spin−orbit splittings are not resolved, and hence each different chemical environment in the Mn 3p signal was fitted with a single peak that comprises the unresolved doublet.

Spectrum *a* in Figure 3 depicts the Mn 3p XPS signal for the as-prepared LMO electrode after Ar^+ sputtering and annealing at 350 °C until the carbon surface contamination has reached a minimum. A lithium-rich surface is observed from the Li 1s XPS signal. Lithium segregation at the surface after sputtering and heat treatment have been already reported by Eriksson.[27−29] It should be noticed that the Li 1s XPS peak at 54 eV is very close to Mn 3p at 48−51 eV, and the sensitivity factor ratio Li/Mn is very small, i.e., 0.047. Therefore, it was impossible to assess the low lithium surface concentration at different states of lithium insertion, and thus the Mn(III) and Mn(IV) surface concentrations were taken as figure of merit.

A broad Mn 3p peak can be fitted with two Gaussian−Lorenzian (70:30) peaks which correspond to Mn(III) and Mn(IV) centered at 48.6 and 50.3 eV, respectively. The latter corresponds to the peak position observed for a reference of MnO_2 (Figure 3h). A similar population of both Mn(III) and Mn(IV) corresponds to a stoichiometry of $Li_xMn_2O_4$ close to $x = 1$.

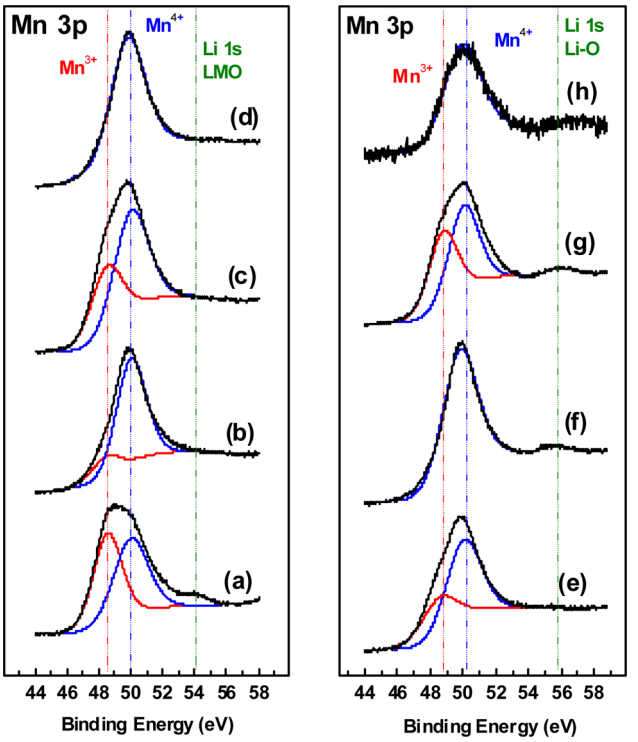

Figure 3. Mn 3p XPS signal of $LiMn_2O_4$ electrode under electrode potential control in 0.1 M $LiNO_3$ for Li^+ extraction at 1.1 V and release at 0.4 V in 0.1 M KNO_3 solution (a) after Ar^+ sputtering and annealing; (b) first extraction (74 mC·cm^{-2}); (c) first insertion (23 mC·cm^{-2}); (d) second extraction; (e) second insertion in 0.1 M $LiNO_3$ + 0.1 M $NaNO_3$ (12 mC·cm^{-2}); (f) third extraction (71 mC·cm^{-2}); (g) third insertion in 0.1 M $LiNO_3$ and 1 M $NaNO_3$ (48 mC·cm^{-2}); (h) MnO_2 reference signal.

Then, the electrode was polarized at 1.1 V for 3 h to release the lithium ions in the lattice (anodic charge of 74 mC·cm^{-2}). The Mn 3p XPS signal is shown in spectrum b in Figure 3 with a predominant Mn(IV) peak and a small proportion of Mn(III). Subsequently, an electrochemical lithium insertion at 0.4 V yielded the peak shown in spectrum c with a relative increase in the Mn(III) peak. Here we should note that we limited the lower potential to 0.4 V in order to avoid the phase equilibrium between $LiMn_2O_4$ and $Li_2Mn_2O_4$ which would lead to Mn(II) dissolution by disproportion of Mn(III) at the electrode surface. The following lithium extraction step at 1.1 V shows an almost complete conversion to Mn(IV) at the surface as shown in spectrum d. The next lithium insertion into the LMO electrode was performed in an electrolyte now containing 0.1 M $LiNO_3$ and 0.1 M $NaNO_3$ with partial recovery of the Mn(III) component of the Mn 3p XPS signal (spectrum e), which upon oxidation at 1.1 V exhibits a completely delithiated surface (spectrum f). This surface could be further lithiated at 1.1 V which resulted in the Mn 3p peak in spectrum *g* with both surface Mn(III) and Mn(IV) components.

The O 1s XPS signals for lithium extraction and insertion are shown in Figure 4 for the experiments a−d in Figure 3. Two peaks centered at 529 and 531 eV are seen which can be related to surface O in Mn octahedral sites and in lithium-containing tetrahedral sites, respectively.[28−31] Notice that the XPS spectra do not change with insertion/extraction cycles. Moreover, the ratio O to Mn was approximately 1.9 to 2.1 for different lithium

DOI: 10.1021/acs.jpcc.5b11722
J. Phys. Chem. C XXXX, XXX, XXX−XXX

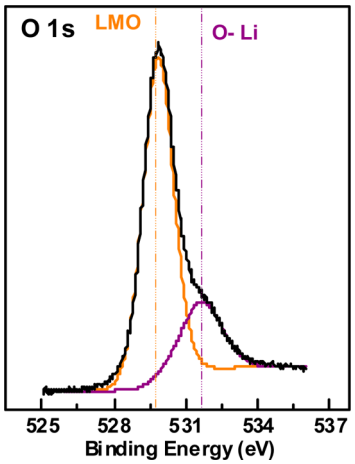

Figure 4. O 1s XPS signal of the $LiMn_2O_4$ electrode in 0.1 M $LiNO_3$ after several extraction/insertion cycles.

contents as expected for $LiMn_2O_4$ stoichiometry. Therefore, no changes in the oxide atom composition are observed on the surface during oxidation and reduction cycles.

The electron configuration of octahedral Mn(III) is $3d^4$ ($3t_{2g}$, $1e_g$), while Mn(IV) is $3d^3$ ($3t_{2g}$). Direct confirmation of the presence of surface Mn(III) species upon lithium insertion has been obtained by UPS experiments, and the results are shown in Figure 5 in the region of Mn t_{2g} and e_g d electrons.[31] The

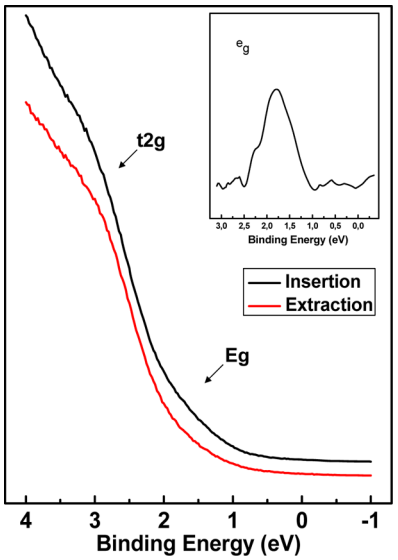

Figure 5. Figure 3a shows the full spectrum, while Figure 3b zooms only the d-orbitals region. The baseline-corrected difference between the spectra of the lithiated and delithiated surface is shown in the inset.

wide UPS spectrum of $LiMn_2O_4$ (0−14.5 eV) shown in the Supporting Information is similar to the spectra reported elsewhere,[30,31] and it is also indicative of a very clean $LiMn_2O_4$ surface.

The difference between the UPS signals for the lithiated (0.4 V) and delithiated (1.1 V) surfaces exhibits a peak in the e_g region as shown in the inset of Figure 5 which is direct evidence of the existence of Mn(III) e_g d electrons in reduced electrode surfaces.

The Li 1 s XPS signal has a very low cross section, and it could only be seen in the as-prepared surface and as a small peak in spectra f and g of Figure 3. Interestingly the Na 1s XPS peak, which can be clearly seen in these experiments, shows no surface sodium in the background experiment for LMO electrodes treated in 0.1 M $LiNO_3$ electrolyte. However, when the electrolyte contained Na^+ the presence of adsorbed sodium on the LMO electrode surface could be observed with larger surface concentration for the 10:1 Na to Li ratio as compared with 1:1 Na to Li ratio in Figure 6. XPS experiments

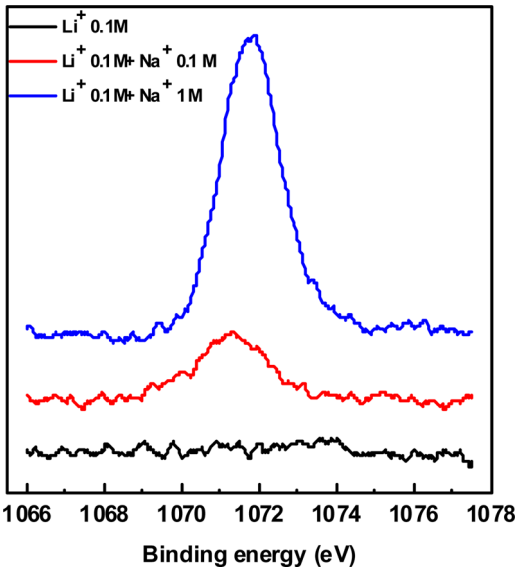

Figure 6. Na 1s XPS signal for $LiMn_2O_4$ electrode in 0.1 M $LiNO_3$, 0.1 M $LiNO_3$ + 0.1 M $LiNO_3$, and 0.1 $LiNO_3$ + 1 M $LiNO_3$.

only probe within 1−3 nm in depth at the surface, and therefore only sodium ions adsorbed at the oxide/electrolyte double layer can be assessed. It is very relevant for the lithium-ion insertion kinetics, the competition of lithium and sodium cations adsorbed at the oxide/electrolyte interface observed by XPS, which would influence the rate of lithium-ion intercalation by blocking surface adsorption sites for lithium as suggested in electrochemical experiments with larger overpotential in CV and smaller lithium insertion charge in brine solutions.

Lithium-Ion Exchange (Insertion and Release). Cyclic voltammetry (Figure 2) has shown that $Li_xMn_2O_4$ can exchange Li^+ ions with aqueous lithium electrolyte and natural brine as is the case with nonaqueous electrolytes, while XPS and UPS have shown the changes in Mn(III)/Mn(IV) surface composition during LiCl extraction/insertion full cycles and the competitive adsorption of Na^+ on the oxide surface.

The potential range explored in the present work (0.4−1.1 V vs Ag/AgCl, 3 M KCl) limits the Li^+ insertion to the composition $0 \leq x \leq 1$ within the tetrahedral sites in the $Li_xMn_2O_4$ spinel framework with high mobility of Li^+ in the 3D interstitial space of the close-packed O^{2-} from λ-MnO_2 to $LiMn_2O_4$.[32] By controlling the cathode potential above 0.4 V we avoid crossing the Li-occupation range above $x > 1$ with shift from tetrahedral to octahedral site occupancy into the phase transition $LiMn_2O_4/Li_2Mn_2O_4$ around 0 V.

On the other hand, unlike the early work of Kanoh[1,2] with λ-MnO_2 cathode/Pt anode, in our hands the polypyrrole (PPy) chloride reversible anode avoids the evolution of chlorine and oxygen in the oxidation step. Therefore, the reversible lithium extraction/release cycle takes place at low cell operation voltage, i.e., <1 V, as will be discussed below.

DOI: 10.1021/acs.jpcc.5b11722
J. Phys. Chem. C XXXX, XXX, XXX−XXX

Chronoamperometry in oxidation and reduction potential steps to 1.1 and 0.6 V, respectively, results in current transients depicted in Figure 7 controlled by the diffusion of Li^+ in the

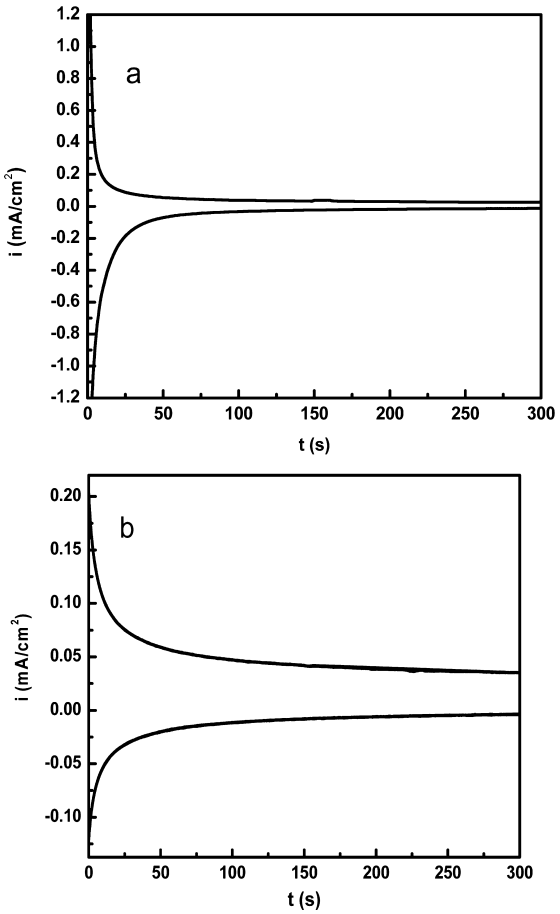

Figure 7. Chronoamperometry of PLD-deposited $LiMn_2O_4$ electrode for release (1.1 V) and insertion (0.6 V) of Li^+ in (a) 0.1 $LiNO_3$ and (b) natural brine.

solid oxide for 0.1 M $LiNO_3$ (A) and natural brine (B). Faster diffusion of hydrated lithium ions in the aqueous electrolyte toward the $Li_xMn_2O_4$ electrode leads to loss of the hydration shell and Li^+ adsorption at surface tetrahedral sites with further Li-ion diffusion into the interstitial space of the host LMO oxide.

The polypyrrole counter electrode potential varies only a few millivolts during the complete intercalation and extraction cycles in natural brine as shown in the Supporting Information for chronoamperometry.

As for cyclic voltammetry the anodic and cathodic charges in natural brine are less than in 0.1 M $LiNO_3$ solution probably due to coadsorption of sodium as revealed by XPS blocking adsorption sites for lithium ions. The state of the surface is expected to determine the exchange of Li as shown by Aurbach[33] in nonaqueous electrolyte.

For one-dimensional semi-infinite diffusion of lithium ions in the PLD $LiMn_2O_4$ thin film the Cottrell equation[34] predicts at long times a linear dependence I vs $t^{-1/2}$ with zero intercept for diffusion length much less than the film thickness, ($\sqrt{(Dt)} \ll l$).

However, this analysis on the current transients for potential steps during lithium extraction/insertion from/into $LiMn_2O_4$ results in an intercept at the $t^{-1/2}$ axis at $I = 0$. This behavior corresponds to the development of a Li^+ concentration profile with diffusion length in the time scale where a linear $I-t^{-1/2}$ relationship is observed comparable to the crystal size or film thickness. Inspection of the $LiMn_2O_4$ nanocrystals in the PLD film shows in Figure 1 an average size of 100 nm.

Van Buren and co-workers[35] have proposed a model for a three-dimensional isotropic diffusion process inside each nanocrystal and time bounded because of the small size of the crystals. Unlike one-dimensional semi-infinite diffusion the straight line does not pass through the origin, but for bounded three-dimensional diffusion the line intercepts at the $t^{-1/2}$ axis at values which are specific for the form of the particle in which diffusion takes place (i.e., 1.77 for sphere and 2.26 for a cube).

The current dependence on time follows

$$I = \frac{FADC_{\mathrm{Li}}^{0}}{a} f(\lambda) \tag{5}$$

where A is the true surface area of contact between the $LiMn_2O_4$ crystal surface and the aqueous electrolyte; $C_{\mathrm{Li}}{}^0$ is the surface concentration of lithium ions after application of the potential step; a is a geometric factor; and $f(\lambda)$ is a function of the crystal geometry and time.[35] The intersection at $t^{-1/2}$ reflects the interference of diffusion profiles in three dimensions. The theory predicts the relationship

$$\lambda = \frac{a}{\sqrt{D_i t}} \tag{6}$$

where the geometric factor is $\lambda = 1.77$ for a sphere and 2.26 for a cube; a is the crystal size dimension, i.e., the spherical particle radius, which in three dimensions for a rectangular parallelepiped corresponds to a, b, and c; and t is the time at which $I = 0$ and the straight line intercepts at $t^{-1/2}$. When an experimental plot of I vs $t^{-1/2}$ contains a straight part the extrapolation of this straight part gives the value of t needed in eq 6.

Figure 8 depicts I vs $t^{-1/2}$ plots for data in Figure 7 for 0.1 M $LiNO_3$ and natural brine with high concentration of sodium chloride, respectively. From the intercepts at $t^{-1/2}$ of the linear portions of these plots and the average particle dimension a = 100 nm and taking an average $\lambda = 2.0$ between a sphere and a cube, we have obtained average diffusion coefficients for insertion and extraction of Li ions, $D_{\mathrm{Li}}{}^+ = 8.4 \times 10^{-10}$ cm^2 s^{-1} in 0.1 M $LiNO_3$ and $D_{\mathrm{Li}}{}^+ = 6.0 \times 10^{-10}$ for natural brine, respectively.

These values are in good agreement with values reported in the literature for lithium insertion/extraction from/to non-aqueous electrolyte batteries. Guyomard and Tarascon reported chemical diffusion coefficients of Li^+ in $LiMn_2O_4$ determined by PITT experiments, to be independent of composition $0 \le x \le 1$ and of the order of 10^{-9} cm^2·s^{-1} for the LMO electrodes in contact with $LiClO_4$ in EC + DEE organic electrolyte.[36] Recently Zhao et al. reported a Li^+ diffusion coefficient in $LiMn_2O_4$ of 5×10^{-10} cm^2·s^{-1} determined by galvanostatic intermittent titration technique (GITT) experiments for $LiMn_2O_4$ in contact with $LiPF_6$ in ethylene carbonate (EC) and diethylcarbonate (DEC) organic electrolyte.[37]

It is to be noticed that the slopes of the $I-t^{-1/2}$ linear plots are given by $F\pi^{1/2}AD_{\mathrm{Li+}}{}^{1/2}C_{\mathrm{Li}}{}^0$, but A is difficult to evaluate. Also the surface concentration of lithium ions, $C_{\mathrm{Li}}{}^0$, is not known. These values are not needed in the method of van Buren et al. since $D_{\mathrm{Li}}{}^+$ is extracted from the value of t extrapolated at $I = 0$.[35]

DOI: 10.1021/acs.jpcc.5b11722
J. Phys. Chem. C XXXX, XXX, XXX−XXX

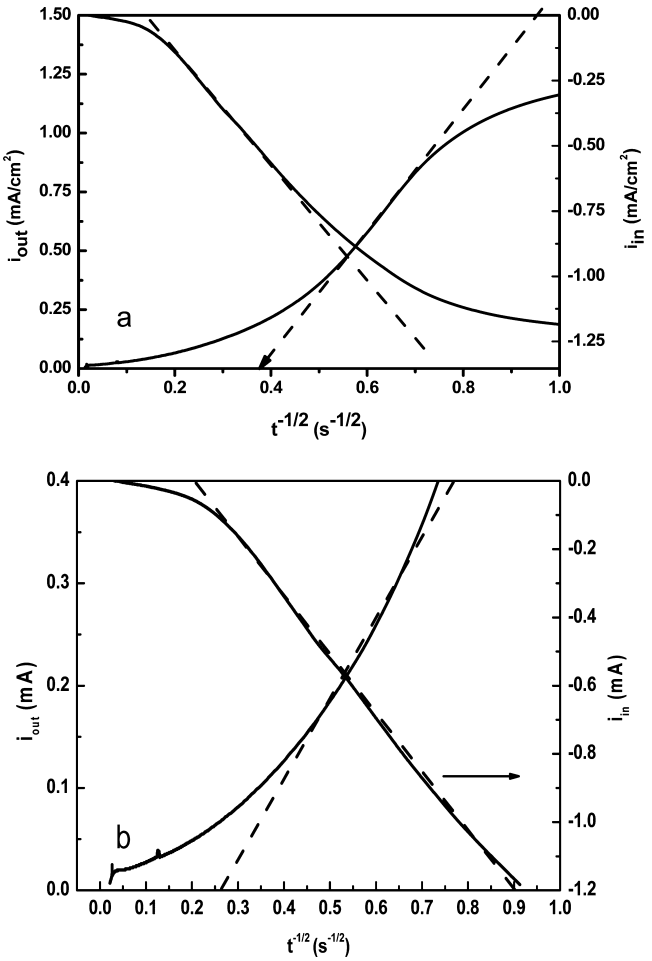

Figure 8. Cottrell plot I vs $t^{-1/2}$ for data in Figure 7.

Good reversibility and stability over a number of cycles have been obtained with the LMO/PPy cell, as shown by the galvanostatic intermittent titration technique (GITT) carried out with electrodes obtained by deposition of a slurry of the $LiMn_2O_4$ mixed oxide, Vulcan carbon black, and PVDF binder. The $Li_xMn_2O_4$/PPy cell was charged and discharged at a constant current of 0.5 mA for 10 s followed by a relaxation time of 30 s. The full GITT processes during charge (delithiation) and discharge (Li^+ intercalation) are shown in Figure 9. We have limited the potential to 0.6 and 1.1 V (3.82−4.32 V vs Li/Li^+). They show a characteristic two voltage plateau at 0.77 and 0.90 V during charge and discharge, respectively (Figure 9), which corresponds to the CV peaks in Figure 2, in good agreement with literature values in nonaqueous electrolyte.[36,37] The transition takes place at x = 0.5 for $Li_{0.5}Mn_2O_4$.

During the Li-ion intercalation into the oxide and extraction into the electrolyte the electrode potential of the PPy counter electrode (anode/cathode electrode area 10:1) only varied a few millivolts (see current transients in Supporting Information) which therefore behaves as a very good chloride-reversible electrode with great stability over a large number of cycles.

Within the phase diagram of Li−Mn−O[38] some layer oxides are known to intercalate sodium ions. In natural brines the ratio Na:Li can be as high as 25:1, and therefore the possibility of Na^+ intercalation should be evaluated. Cyclic voltammetry of $LiMn_2O_4$ in $NaNO_3$ and NaCl shows anodic peaks for the release of Li ions but negligible current in the reverse reduction

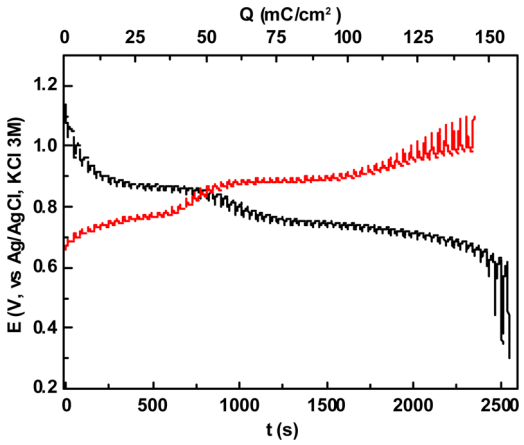

Figure 9. GITT of an electrode prepared by deposition of a slurry of $LiMn_2O_4$ (8% w/w), Vulcan carbon (10%), and PVDF (10%) in *N*-methylpyrrolidone on Ccrbon (Poco) dried at 105 °C and 0.5 mA·cm^{-2}.

scan which suggests that sodium ions cannot be intercalated (see CV in Supporting Information).

In situ X-ray diffraction pattern of $Li_xMn_2O_4$ spinel cathode material (within $0 \leq x \leq 1$) during oxidation obtained in synchrotron as the X-ray source has been reported to shift the reflections to higher 2θ values as the electrode is delithiated.[39] The spectra in Figure 10 show the comparison in the present

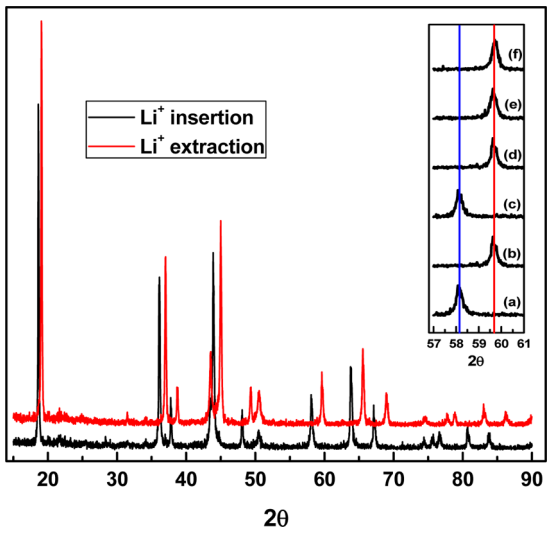

Figure 10. XRD pattern of an electrode prepared by deposition of a slurry of $LiMn_2O_4$ (8% w/w), Vulcan carbon (10%), and PVDF (10%) in *N*-methylpyrrolidone on stainless steel, before and after oxidation (extraction). Inset: Evolution of the $2\theta \sim 57-61$ range (see text).

study of the as-prepared $LiMn_2O_4$ with the electrode after 2 h polarization at 1.1 V. A shift of the LMO reflections to larger 2θ values can be clearly identified with all peaks moving to higher angles in a continuous fashion during charge at 1.1 V as compared to the initial $LiMn_2O_4$ electrode. The calculated lattice constant of the cubic unit cell, based on the position of (531) peak, contracted from 8.25 Å for the uncharged (lithiated LMO) cell to 8.07 Å for the fully charged cell.

The inset in Figure 10 shows the evolution of the LMO XRD reflections in the 2θ range 58−60° for the initial electrode (a) and after the first and second (b−d) insertion/extraction cycles

DOI: 10.1021/acs.jpcc.5b11722
J. Phys. Chem. C XXXX, XXX, XXX−XXX

in 0.1 M $LiNO_3$ solution with a clear shift in the peak position which reflects the Li^+ insertion in the bulk oxide. Note, however, in the next oxidation and further reduction steps in lithium-free 1 M $NaNO_3$ that there is no variation in the peak position (e–f); therefore, no intercalation of sodium ions into the LMO lattice takes place.

CONCLUSIONS

Selective extraction of LiCl from natural salt lake brines can be accomplished using an electrochemical method based on $LiMn_2O_4$ (LMO) lithium intercalation electrode and polypyrrole (PPy) reversible chloride electrode.

The surface and bulk chemistry of $Li_xMn_2O_4$ ($0 \leq x \leq 1$) obtained by pulsed laser deposited (PLD) thin films and composite LMO/carbon black electrodes was studied by cyclic voltammetry, XPS/UPS, XRD, chronoamperometry, and galvanostatic intermittent transient titration (GITT) experiments in model $LiNO_3$ solutions and natural brines from Salar de Olaroz (Jujuy, Argentina).

The surface study of $Li_xMn_2O_4$ by photoelectron spectroscopy, XPS, and UPS showed Mn/O surface stoichiometry close to 1:2 and 1:1 Mn^{IV}/Mn^{III} ratio for the as-prepared material, with Mn^{III} depletion during oxidation at 1.1 V and recovery of surface Mn^{III} after reduction at 0.4 V. Coadsorption of Na^+ was detected which resulted in slower intercalation Li-ion flux, but XRD evidence shows that Na^+ cannot be intercalated in the Mn oxide electrode in the potential window 0.4–1.1 V.

Repetitive CV and GITT experiments showed reversible extraction/intercalation of Li ions in LMO with high selectivity and electrode stability in natural brine, while PPy is reversible to chloride ions.

Chronoamperometry for time-bound diffusion in small nanocrystals with interference of concentration profiles yielded chemical diffusion coefficients $D_{Li^+} \sim 10^{-10}$ $cm^{-2}\cdot s^{-1}$ in agreement with previous studies in nonaqueous electrolytes.

The theoretical charge capacity of $LiMn_2O_4$ is 147 mAh/g, while the theoretical maximum mass of Li recovered per gram of mixed spinel oxide is only 39 mg/g. It has been observed that some oxide particles agglomerate resulting in carbon and oxide segregation on the surface which may result in poor electrical contact with the current collector and thus in a lower efficiency for lithium recovery. To achieve the theoretical mass of Li recovered per gram of mixed spinel oxide would require very good oxide particle-to-carbon black particle ratio and an even lower efficiency for lithium recovery. For instance, Kanoh et al. have reported 11 mg/g of λ-MnO_2.[2] Since lithium is the lightest metal it can store much charge per unit mass, but the "lithium paradox" is that small mass can be recovered by each Faraday of charge, and therefore the engineering design of the recovery reactor would be a key factor.

ASSOCIATED CONTENT

Supporting Information

The Supporting Information is available free of charge on the ACS Publications website at DOI: 10.1021/acs.jpcc.5b11722.

Ppy CV, wide XPS spectrum, Mn 3s and Mn 2p XPS signals for experiments in Figure 3; electron energy levels of LMO; UPS wide spectra for oxidized and reduced LMO; current transients and PPy electrode potential (PDF)

AUTHOR INFORMATION

Corresponding Author

*E-mail: calvo@qi.fcen.uba.ar.

Present Address

†Comisión Nacional de Energía Atómica. Physics. Condensed Matter. Centro Atómico Constituyentes. Gral. Paz 1499 (1650) San Martín, Argentina. San Martin, Provincia de Buenos Aires, AR 1450. + 54 11 67727059; rubi@tandar.cnea.gov.ar.

Author Contributions

The manuscript was written through contributions of all authors. All authors have given approval to the final version of the manuscript.

Notes

The authors declare no competing financial interest.

ACKNOWLEDGMENTS

Funding from CONICET and ANPCyT PICT 2012 No. 1452 and FS-Nano 07 and research doctoral and postdoctoral fellowships from CONICET by FM and from ANCPCyT (M. del P) are gratefully acknowledged. D.R. acknowledges support from CONICET-PIP 291 and CIC-Buenos Aires Province, (Argentina).

REFERENCES

(1) Kanoh, H.; Ooi, K.; Miyai, Y.; Katoh, S. Selective Electroinsertion of Lithium Ions into a Pt/Λ-MnO_2 Electrode in the Aqueous Phase. *Langmuir* **1991**, *7*, 1841–1842.

(2) Kanoh, H.; Ooi, K.; Miyai, Y.; Katoh, S. Electrochemical Recovery of Lithium Ions in the Aqueous Phase. *Sep. Sci. Technol.* **1993**, *28*, 643–651.

(3) Pasta, M.; Battistel, A.; La Mantia, F. Batteries for Lithium Recovery from Brines. *Energy Environ. Sci.* **2012**, *5*, 9487–9491.

(4) Trocoli, R.; Battistel, A.; La Mantia, F. Selectivity of a Lithium-Recovery Process Based on $LiFePO_4$. *Chem. - Eur. J.* **2014**, *20*, 9888–9891.

(5) Trocoli, R.; Battistel, A.; La Mantia, F. Nickel Hexacyanoferrate as Suitable Alternative to Ag for Electrochemical Lithium Recovery. *ChemSusChem* **2015**, *8*, 2514–2519.

(6) Lee, J.; Yu, S.-H.; Kim, C.; Sung, Y.-E.; Yoon, J. Highly Selective Lithium Recovery from Brine Using a Lambda-MnO_2-Ag Battery. *Phys. Chem. Chem. Phys.* **2013**, *15*, 7690–7695.

(7) Kim, S.; Lee, J.; Kang, J. S.; Jo, K.; Kim, S.; Sung, Y.-E.; Yoon, J. Lithium Recovery from Brine Using a Lambda-MnO_2/Activated Carbon Hybrid Supercapacitor System. *Chemosphere* **2015**, *125*, 50–56.

(8) Hoshino, T. Development of Technology for Recovering Lithium from Seawater by Electrodialysis Using Ionic Liquid Membrane. *Fusion Eng. Des.* **2013**, *88*, 2956–2959.

(9) Hoshino, T. In *Lithium Recovery from Seawater by Electrodialysis Using Ionic Liquid-Based Membrane Technology*, ECS Transactions, The Electrochemical Society: Pennington, NY, 2013; pp 173–177.

(10) Intaranont, N.; Garcia-Araez, N.; Hector, A. L.; Milton, J. A.; Owen, J. R. Selective Lithium Extraction from Brines by Chemical Reaction with Battery Materials. *J. Mater. Chem. A* **2014**, *2*, 6374–6377.

(11) Liu, X.; Chen, X.; Zhao, Z.; Liang, X. Effect of Na^+ on Li Extraction from Brine Using $LiFePO_4$/$FePO_4$ Electrodes. *Hydrometallurgy* **2014**, *146*, 24–28.

(12) Calvo, E. J.; Marchini, F. Electrochemically Extracting Lithium from E.G. Sea Water, Comprises Contacting Electrodes with the Solution, Applying Voltage or Circulating Current to Electrodes, Exchanging Solution with Dilute Solution, and Reversing Electrical Polarity. US2014076734-A1; WO2014047347-A1; AU2013317990-A1; AR92617-A1; US2015252485-A1, 2013.

DOI: 10.1021/acs.jpcc.5b11722
J. Phys. Chem. C XXXX, XXX, XXX–XXX

(13) Marchini, F.; Herrera, S.; Torres, W.; Tesio, A. Y.; Williams, F. J.; Calvo, E. J. Surface Study of Lithium-Air Battery Oxygen Cathodes in Different Solvent-Electrolyte Pairs. *Langmuir* **2015**, *31*, 9236−9245.
(14) Rossouw, M.; de Kock, A.; de Picciotto, L.; Thackeray, M.; David, W.; Ibberson, R. Structural Aspects of Lithium-Manganese-Oxide Electrodes for Rechargeable Lithium Batteries. *Mater. Res. Bull.* **1990**, *25*, 173−182.
(15) Rougier, A.; Striebel, K. A.; Wen, S. J.; Cairns, E. J. Cyclic Voltammetry of Pulsed Laser Deposited Li$_x$Mn$_2$O$_4$ Thin Films. *J. Electrochem. Soc.* **1998**, *145*, 2975−2980.
(16) Shokoohi, F. K.; Tarascon, J. M.; Wilkens, B. J.; Guyomard, D.; Chang, C. C. Low Temperature LiMn$_2$O$_4$ Spinel Films for Secondary Lithium Batteries. *J. Electrochem. Soc.* **1992**, *139*, 1845−1849.
(17) Guyomard, D.; Tarascon, J. M. Rocking-Chair or Lithium-Ion Rechargeable Lithium Batteries. *Adv. Mater.* **1994**, *6*, 408−412.
(18) Guyomard, D.; Tarascon, J. M. Rechargeable Li$_{1+X}$Mn$_2$O$_4$ carbon Cells with a New Electrolyte Composition. *J. Electrochem. Soc.* **1993**, *140*, 3071−3081.
(19) Tarascon, J. M.; Guyomard, D. Li Metal-Free Rechargeable Batteries Based on Li$_{1+X}$Mn$_2$O$_4$ Cathodes ($0 \leq X \leq 1$) and Carbon Anodes. *J. Electrochem. Soc.* **1991**, *138*, 2864−2868.
(20) Ooi, K.; Miyai, Y.; Katoh, S.; Maeda, H.; Abe, M. Topotactic Li+ Insertion to Λ-MnO$_2$ in the Aqueous Phase. *Langmuir* **1989**, *5*, 150−157.
(21) Doblhofer, K.; Rajeshwar, K., Electrochemistry of Conducting Polymers. In *Handbook of Conducting Polymers*; Skotheim, T. A., Elsenbaumer, R. L., Reynolds, J. R., Eds.; Marcel Dekker: New York, 1998; Vol. *1*, pp 531−588.
(22) Feldberg, S. W. Reinterpretation of Polypyrrole Electrochemistry. Consideration of Capacitive Currents in Redox Switching of Conducting Polymers. *J. Am. Chem. Soc.* **1984**, *106*, 4671−4674.
(23) Oku, M.; Hirokawa, K.; Ikeda, S. X-Ray Photoelectron Spectroscopy of Manganese-Oxygen Systems. *J. Electron Spectrosc. Relat. Phenom.* **1975**, *7*, 465−473.
(24) Cerrato, J. M.; Hochella, M. F., Jr; Knocke, W. R.; Dietrich, A. M.; Cromer, T. F. Use of XPS to Identify the Oxidation State of Mn in Solid Surfaces of Filtration Media Oxide Samples from Drinking Water Treatment Plants. *Environ. Sci. Technol.* **2010**, *44*, 5881−5886.
(25) Kochur, A. G.; Kozakov, A. T.; Nikolskii, A. V.; Googlev, K. A.; Pavlenko, A. V.; Verbenko, I. A.; Reznichenko, L. A.; Krasnenko, T. I. Valence State of the Manganese Ions in Mixed-Valence La$_{1-\alpha}$Bi$_\beta$Mn$_{1+\delta}$O$_{3\pm\gamma}$ Ceramics by Mn 2p and Mn 3s X-Ray Photoelectron Spectra. *J. Electron Spectrosc. Relat. Phenom.* **2012**, *185*, 175−183.
(26) Kochur, A. G.; Kozakov, A. T.; Nikol'skii, A. V.; Guglev, K. A.; Pavlenko, A. V.; Verbenko, I. A.; Reznichenko, L. A.; Shevtsova, S. I. Valence State of Manganese Ions in the La$_{1-\alpha}$Bi$_\beta$Mn$_{1+\delta}$O$_{3\pm\gamma}$ Ceramics. *Phys. Solid State* **2013**, *55*, 743−747.
(27) Eriksson, T. Limn2o4 as a Li-Ion Battery Cathode. From Bulk to Electrolyte Interface. *Comprehensive Summaries of Uppsala Dissertations from the Faculty of Science and Technology 651*. 53 pp., Faculty of Science and Technology, Uppsala University, Uppsala, Sweeden, 2001.
(28) Eriksson, T.; Andersson, A. M.; Bishop, A. G.; Gejke, C.; Gustafsson, T.; Thomas, J. O. Surface Analysis of LiMn$_2$O$_4$ Electrodes in Carbonate-Based Electrolytes. *J. Electrochem. Soc.* **2002**, *149*, A69−A78.
(29) Eriksson, T.; Gustafsson, T.; Thomas, J. O. Surface Structure of Limn2o4 Electrodes. *Electrochem. Solid-State Lett.* **2002**, *5*, A35−A38.
(30) Wu, Q.-H. Photoelectron Spectroscopy of Intercalation Phases: Na and Li in V2o5 Thin Films and LiMn$_2$O$_4$. PhD, Darmstadt University of Technology, Darmstadt, 2003.
(31) Wu, Q. H.; Thissen, A.; Jaegermann, W. Photoemission Spectroscopy and Electronic Structures of LiMn$_2$O$_4$. *Chin. Phys. Lett.* **2006**, *23*, 2202−2205.
(32) Goodenough, J. B.; Manthiram, A. A Perspective on Electrical Energy Storage. *MRS Commun.* **2014**, *4*, 135−142.
(33) Aurbach, D.; Gamolsky, K.; Markovsky, B.; Salitra, G.; Gofer, Y.; Heider, U.; Oesten, R.; Schmidt, M. The Study of Surface Phenomena Related to Electrochemical Lithium Intercalation into Li$_x$Mo$_y$ Host Materials (M = Ni, Mn). *J. Electrochem. Soc.* **2000**, *147*, 1322−1331.
(34) Bard, A. J.; Faulkner, L. R. *Electrochemical Methods. Fundamentals and Applications*, 2nd ed.; J. Wiley: New York, 2001.
(35) van Buren, F. R.; Broers, G. H. J.; Bouman, A. J.; Boesveld, C. An Electrochemical Method for the Determination of Oxygen Ion Diffusion Coefficients in La$_{1-X}$Sr$_x$CoO$_{3-y}$ Compounds Theoretical Aspects. *J. Electroanal. Chem. Interfacial Electrochem.* **1978**, *87*, 389−394.
(36) Guyomard, D.; Tarascon, J. M. Li Metal-Free Rechargeable Limn2o4/Carbon Cells - Their Understanding and Optimization. *J. Electrochem. Soc.* **1992**, *139*, 937−948.
(37) Zhao, X.; Reddy, M. V.; Liu, H.; Ramakrishna, S.; Rao, G. V. S.; Chowdari, B. V. R. Nano LiMn$_2$O$_4$ with Spherical Morphology Synthesized by a Molten Salt Method as Cathodes for Lithium Ion Batteries. *RSC Adv.* **2012**, *2*, 7462−7469.
(38) Paulsen, J. M.; Dahn, J. R. Phase Diagram of Li-Mn-O Spinel in Air. *Chem. Mater.* **1999**, *11*, 3065−3079.
(39) Yang, X. Q.; Sun, X.; Lee, S. J.; McBreen, J.; Mukerjee, S.; Daroux, M. L.; Xing, X. K. In Situ Synchrotron X-Ray Diffraction Studies of the Phase Transitions in Li$_x$Mn$_2$O$_4$ Cathode Materials. *Electrochem. Solid-State Lett.* **1999**, *2*, 157−160.

DOI: 10.1021/acs.jpcc.5b11722
J. Phys. Chem. C XXXX, XXX, XXX−XXX